Improvement of Mechanical and Corrosion Properties of Weld in Stainless Steel in Crude Oil Tank by Using Nano-Fillers / Original article

Researcher Ali Abdulzahra Shanshoon

Azad Islamic University – Dept. of Production and Manufacturing,
Islamic Republic of Iran
engalialkorji2@gmail.com

تحسين الخواص الميكانيكية وخصائص التأكل للحام الفولاذي المقاوم للصدأ في خزان النفط الخام بأستخدام حشوات النانو

الباحث علي عبد الزهرة شنشون

قسم انتاج وتصنيع – جامعة ازاد الاسلامية \ الجمهورية الاسلامية الايرانية

Abstract

The aim of this study is to investigate the corrosion behavior and mechanical properties of welded steel exposed to gases emitted from crude oil reservoirs. In this study, two types of nanoparticles were used as fillers during welding to improve corrosion and mechanical properties. TiO2 and SiO2 nanoparticles were mixed with soldering oil in four mass concentrations of 0, 1, 2.5 and 5% by ultrasonic bath method and used as filler during the welding process. In order to prepare the samples, plain carbon steel with a thickness of 3 mm was used and they were welded together by electric arc welding. Then, characteristics such as mass loss percentage, optical microscope and SEM imaging, polarization corrosion test and tensile and bending test were performed on the samples. Also, this test was used as finite element modeling by Abaqus software. The results of microstructure examination showed that in the weld button, the grain size was smaller due to recrystallization and the grains grew in the longitudinal direction, but the grain size in the base metal area was uniform. The results of the weight loss percentage study showed that the effect of TiO2 nanoparticles in preventing mass loss of the samples was better and the lowest mass loss was observed at a mass percentage of 2.5%. Overall, the results of this study showed that for the use of 2.5% TiO2 nanoparticles as a filler material during welding of plain carbon steel, the corrosion resistance, tensile and flexural strength of the samples improved by 97.38%, 16.67% and 24.19%. The results of the tensile and bending tests showed that the addition of TiO2 nanoparticles during the welding process increased the maximum flexural and tensile strength of the welded samples, so that for the sample with 2.5% nanoparticles, the maximum flexural and tensile strength increased by 10.74% and 9.93%, respectively. Comparison of numerical and experimental modeling results showed that the error of numerical modeling by finite element method in measuring tensile and flexural strength was 13.19% and 9.07%, respectively.

Keywords: Nanofiller, Welding, Microstructure, Mechanical Properties, Corrosion.

المستخلص

تهدف هذه الدراسة الى دراسة سلوك التأكل والخصائص الميكانيكية للصلب الملحوم المعرض للغازات المنبعثة من مكامن النفط الخام . في هذه الدراسة , استخدم نوعان من الجسيمات النانوية كحشوات اثناء اللحام لتحسين التأكل والخصائص الميكانيكية . خلطت جسيمات نانوية من ثاني اوكسيد التيتانيوم (Tio2) وثاني اوكسيد السليون (Sio2) النانوية مع زيت اللحام باربعة تركيزات كتلة وهي (0, 1, 2,5 , 5 %) بطريقة حمام الموجات فوق الصوتية , واستخدمت كحشوة اثناء عملية اللحام لتحضير العينات . استخدم فولاذ كاربوني عادي بسمك (3مم) ولحمت معاً بواسطة اللحام بالقوس الكهربائي . بعد ذلك اجريت على العينة خصائص مثل نسبة فقدان الكتلة والتصوير بالمجهر الضوئي والمجهر الالكتروني الماسح واختبار التأكل بالاستقطاب , واختبار الشد والانحناء كما استخدم هذا الاختبار كنمذجة للعناصر المحدودة بواسطة برنامج Abqus . اظهرت نتائج فحص البنية الدقيقة ان حجم الحبيبات في المنطقة المتأثرة باللحام كانت اصغر بسبب اعادة التبلور وان الحبيبات نمت في الاتجاه الطولي , بينما كان حجم الحبيبات في منطقة المعدن الاساسي موحداً . واظهرت نتائج دراسة نسبة فقدان الوزن ان تأثير جسيمات Tio2 النانوية في منع فقدان كتلة العينة كان افضل , ولوحظ اقل فقدان للكتلة عند نسبة كتلة (2.5%) وبشكل عام اظهرت نتائج هذه الدراسة انه عند استخدام جسيمات Tio2 النانوية بنسبة (2.5%) كمادة حشو اثناء اللحام الفولاذ الكاربوني العادي ادى الى تحسن في مقومة التاكل وقوة الشد والانحناء للعينات بنسبة (% 24.19, 16.67% , 97.38%). اظهرت نتائج اختبارات الشد والانحناء ان اضافة جسيمات نانوية من ثاني اوكسيد التيتانيوم اثناء عملية اللحام قد زادت من اقصى قوة انحناء وشد للعينات الملحومة , بحيث زادت اقصى قوة انحناء وشد للعينة التي تحتوي على 2.5% جسيمات نانوية بنسبة (9.93% و 10.74%) على التوالي . اظهرت مقارنة نتائج النمذجة العددية والتجريبية ان خطأ النمذجة العددية بطريقة العناصر المحدودة في قياس قوة الشد والانحناء كان (9.07% و13.19%) على التوالي .

الكلمات المفتاحية : حشو نانوي , لحام . بنية مجهرية , خصائص ميكانيكة , تأكل .

1-Introduction

Steel is one of the most important materials used in industry. Properties such as strength, corrosion resistance and weldability of steel are very important in the design and manufacture of industrial parts. These capabilities have made the role of steel in industry very prominent. The weldability of steel has led to many important industrial equipment being made by welding steel parts. However, most welded joints have weaker properties than unwelded areas due to defects caused by the high temperature of this process. The mechanical properties and microstructure of the weld are of great importance, which is why extensive research has been conducted today in the fields of inventing new welding processes and improving the performance and service life of welded parts (Baddoo 2008). Research results have shown that the presence of metal oxide nanoparticles of some elements such as zirconium, nickel molybdenum and titanium can cause the formation of a ferrite core (Lucas 1996). Studies by Vimalraj et al. (2016) show that nanoparticles in GMAW and TIG welding have improved the microstructure, mechanical properties and welding physics in plain carbon steel (St37). Abdollahzadeh et al. (2016) studied the effect of adding silicon carbide nanoparticles on the mechanical properties of AZ31 magnesium alloy welded by friction stir welding. In this study, the friction stir welding process was used to perform butt jointing of AZ31 magnesium alloy and simultaneously produce Mg/Sic nanocomposite at the joint. The main reason for these changes is related to the presence of silicon carbide nanoparticles, which contribute to the fineness of the structure by creating a locking effect on grain boundaries, helping to nucleate recrystallized grains, and affecting the fracture of primary grains. Ahmadifard et al. (2018) studied the effect of pass number and ZrO2 nanoparticles on microstructure, mechanical properties, and wear behavior in friction stir welding of Al-5083. In this study, friction stir welding process was used to perform butt joint of 5083 aluminum alloy and simultaneously produce Al-ZrO2 nanocomposite at the joint. Behzadinezhad et al. (2021) studied the modification of mechanical properties of friction stir welding of AM60 magnesium alloy by changing the rotation speed and adding alumina nanoparticles. In this study, mechanical properties of friction stir welding of AM60 alloy were investigated in two cases: without alumina nano-reinforcing particles and with alumina nano-reinforcing particles. Zhao et al. (2017) first produced an Al-Cu-Mg alloy nanocomposite with carbon nanotubes] 1[and then welded the sheets together using a friction stir welding process and reported that by welding, carbon nanotubes were uniformly distributed in the stirring zone, which improved the properties. The aim of this research is to improve the corrosion and mechanical properties of the weld in plain carbon steel by making nanofillers. One of the main problems in the oil and reservoir fields is corrosion caused by various gases inside the reservoirs at the weld. This research aims to increase the corrosion resistance of the weld and also improve the mechanical properties of the weld, and the innovative aspect of this research is the use of nanofillers for this purpose.

2-Materials and Methods

2-1-Samples Created

In this study, the corrosion and mechanical behavior of welded plain carbon steel in the interior of a crude oil tank was investigated. Each sample was cut from a 3 mm steel sheet with dimensions of 2×10 cm2.

2-2-Cleaning operations of steel parts

Before welding, the surface of all samples must be cleaned of any contamination. There are excess particles, grease, soot, etc. on the surface of steel sheets. The purpose of any cleaning operation is to remove these unwanted materials from the surface of the steel sheet. Table 1 describes the methods used in this study to clean the surface of the samples before welding. In the first stage, mechanical cleaning was performed. Then, to remove grease, a cleaning method with chemicals was used. In the last stage, combined mechanical and chemical cleaning was performed to remove additional materials such as paint, etc.

2-3-Welding Method

Using the electric arc welding method, the samples were welded together in a butt joint with and without the presence of nanoparticles. Figure 1 shows a schematic of the process of preparing the samples for welding. In order to butt-join the steel sheets, a V-shaped groove was created as shown in Figure 1. The standard defined for butt-joining is AWS B2.1.

Table 1-Methods used to clean the surface of the samples before welding

Removal and cleaning method	Destructive effect on the weld	Type of disturbing layer
Mechanical cleaning such as brushing or sanding	Stick of the electrode to the part	Surface oxide
Cleaning with a cleaning cloth and cleaning with permitted chemicals	Creation of bubbles in the weld	Grease
Chemical and mechanical cleaning	Weak weld point and improper appearance of the weld	Paint

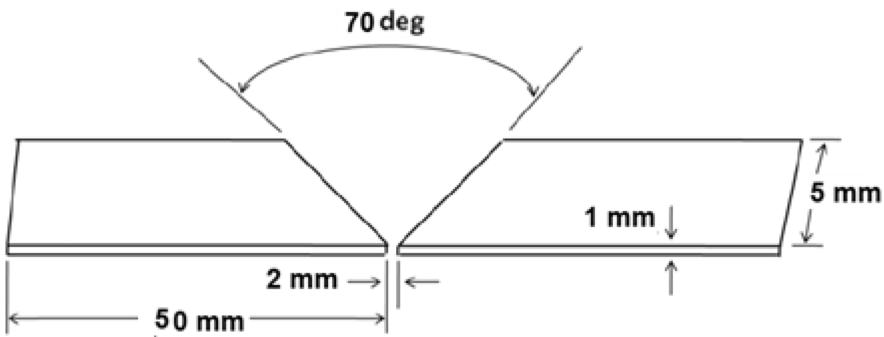

Figure 1- Schematic of butt welding used in this thesis

To connect the created samples, the arc welding method with 110 amps and a voltage of 220 volts was used. The electrode used for connection was E6013.

2-4- Nanoparticles used during the welding process

A review of the research background showed that various nanoparticles have been investigated in the field of welding and improving its properties, but titanium dioxide and silicon dioxide nanoparticles were among the nanoparticles affecting mechanical properties, which were investigated by researchers such as (Golbabaei et al. 2007; Rajeswari et al. 2020; Sabokrouh and Khoshsima 2018; Balos et al. 2019; Giridharan et al. 2022)] 2[. Therefore, in this study, these two nanoparticle models were also used to improve the properties of the weld line. Table 2 presents the technical and physical characteristics of the nanoparticles used in this study. These nanoparticles were obtained from Nanosani Company, Mashhad, Iran.

Table 2- Characteristics of titanium dioxide and silicon dioxide nanoparticles

Chemical formula	TiO2	SiO2
Structure	Powder	Amorphous
Color	White	White
Density	79.87 gr/mol	Hydrophilic
Molecular mass	4.62 gr/cm3	2.4 gr/cm3
Particle size	20 nm	20-30 nm
Percent purity	10-45 m2/gr	above 99%
Country of manufacture	America	America
Chemical formula	TiO2	SiO2

2-5- Method of making nanofiller

Given that the aim of this research is to investigate the effect of adding nanoparticles to the joint area during the welding process, an oil-based filler containing nanoparticles was made for this purpose. The filler in question was made in such a way that it was rubbed into the weld line and the oil quickly evaporated during welding, and the nanoparticles entered the molten weld seam. The base oil used in this research was UST222 industrial soldering oil from Olsols. Given the high specific surface area of nanoparticles, if these nanoparticles are mixed in liquids, they will be strongly absorbed, which will cause the nanoparticles to form clumps and have negative effects on welding. For this purpose, the nanoparticles must be dispersed in the soldering oil under the influence of ultrasonic waves. Given that soldering oil is solid at ambient temperature, it must be converted to a liquid so that the nanoparticles can be easily dispersed in it.

Using a hair dryer, the oil was slowly heated so that it all turned into a liquid. Then, the nanoparticles were added to the melted oil and the dispersion operation was performed using ultrasonic waves and an ultrasonic bath. First, the ultrasonic bath tank was filled with water up to ¼ of its volume. Then, according to Figure 2, the nanoparticles and soldering oil were weighed in the required amount. After the solder oil changed phase from solid to liquid, the nanoparticles were added to the solder oil and placed inside the ultrasonic bath for one hour. The purpose of this work is to evenly distribute the nanoparticles in the solder oil without clumping. After the process of dispersing the nanoparticles in the solder oil was completed, the manufactured sample was immediately transferred to a freezer at a temperature of -19 degrees Celsius and kept there until the test was performed. The purpose of quickly transferring the nanoparticle solution and soldering oil is to prevent the nanoparticles from clumping again.

Before any welding operation, the surface of the joint of two steel sheets was stirred with this nanofiller and then the welding operation was performed. Considering that the soldering oil evaporates quickly during the welding process, the nanoparticles in the nanofiller remain on the weld surface and will be combined with the weld melt.

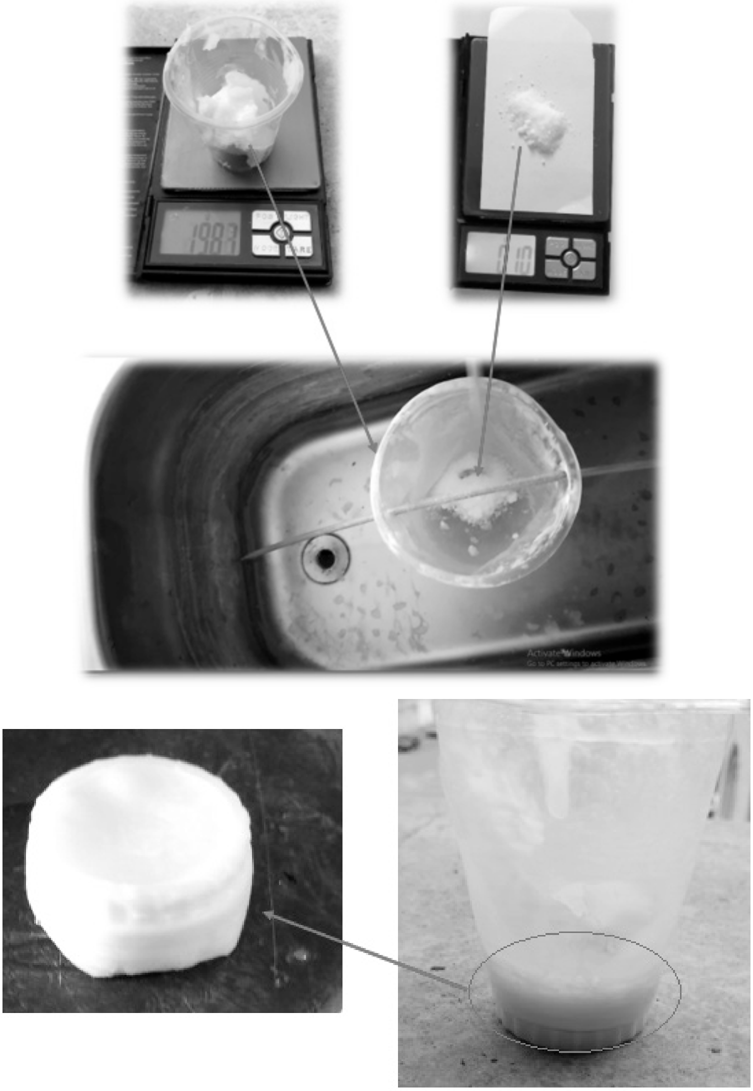

Figure 2- Top: Method of making nanofiller with ultrasonic bath. Bottom: Made nanofiller

2-6- Different mass concentrations of nanoparticles in the filler

Baridula et al2017)] 1 [) and Fattahi] 6[et al. (2015) showed in their research conducted in the last decade that the mass of nanoparticles consumed during the welding process has a significant effect on the mechanical properties and microstructure of the weld, so in this research, several different mass levels of nanoparticles were used. The filler made contains a combination of nanoparticles and soldering oil, and the different amounts used for each nanofiller sample are shown in Table 3. A total of 4 different levels of nanoparticles were used for each type of nanoparticles, including 0%, 1%, 2.5% and 5%. 5% nanoparticles means that in every 10 grams of filler of this nanoparticle, there are 0.5 grams of nanoparticles.

Table 3-Weight composition of different nanofillers made in this research

Label	Mass Precent (%)	Nanoparticle weight (g)	Oil Weight (g)
NanoFiller-0.0%	0	0	10
NanoFiller-1.0%	1	0.1	10
NanoFiller-2.5%	2.5	0.25	10
NanoFiller-5.0%	5	0.50	10

2-7- Placing various welded samples inside the crude oil tank

As is clear from the title of this research, the aim of this thesis is to investigate the effects of gases inside the crude oil tank on the properties of the welded steel plate. For this purpose, the welded samples were placed inside a container and placed inside the crude oil tank. Each sample was placed inside the tank for a period of six hours. Figure 3 shows the chamber intended for installing the welded samples inside it. In fact, this chamber is designed to be installed on the roof of the crude oil tank and the samples inside the chamber are located inside that chamber through a drain. The gases emitted from the crude oil are directly in contact with the samples.

2-8- Experimental tests

In this study, four or five experiments were conducted on each sample. First, the chemical composition of the steel samples was determined. Then, the change in weight of each sample during the time it was placed inside the tank was calculated. Then, their tensile, bending, microstructure, and corrosion resistance were also measured.

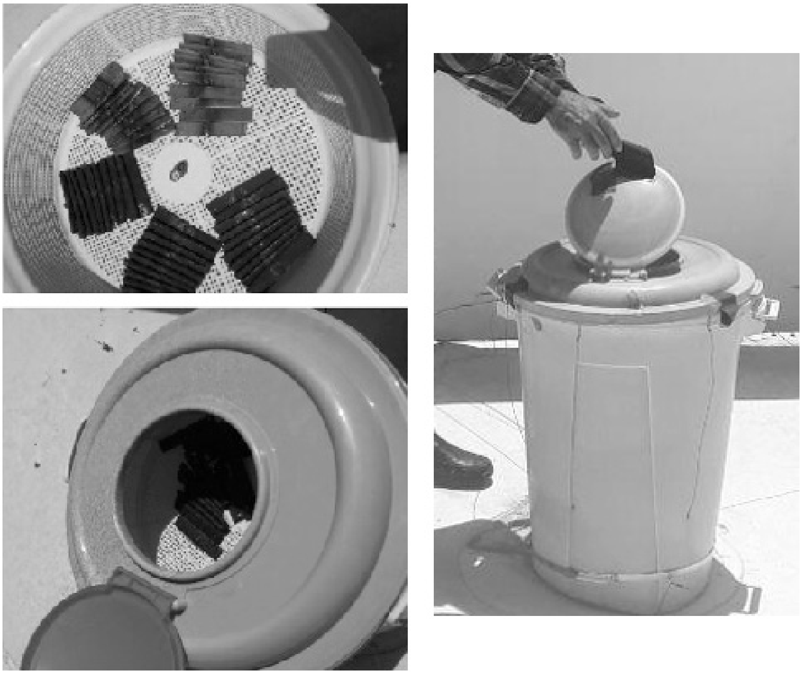

Figure 3-Designed chamber for mounting samples

2-9- Determining the change in sample weight

It should be noted that during the time the samples were inside the tank, they lost weight due to corrosion, so this weight loss was measured using a digital scale model S1202. In order to calculate the percentage of weight loss of the samples, equation 1 was used, in which W1, W2, and RW are the initial weight of the sample, the secondary weight of the sample, and finally the percentage of weight loss, respectively:

$$RW = \left(\frac{W_1 - W_2}{W_1}\right) \times 100 \quad \textbf{(1)}$$

2-10- Investigation of the microstructure of the weld

In order to investigate the microstructure of the weld, two imaging methods were used, with an optical microscope and a scanning electron microscope (SEM). These two imaging methods were used to determine the presence of impurities at the weld line junction in different areas of the weld line.

2-11- Tensile and flexural tests

The two main mechanical properties for each part include flexural and tensile strength. In this study, these two properties were measured for different samples8[ ]. The standards for performing tensile and flexural tests are ASTM E290 and ASTM E858, respectively. Figure 4 shows the device for performing tensile and flexural tests. The Centam STM-50 is the device that was used for this purpose, and by changing the jaws of the device, both tests were performed by it.

2-12-Polarization corrosion test

The polarization test is used to investigate corrosion behavior, find corrosion rates, investigate active-passive behavior, corrosion potential, protection potential and pitting potential of different welding areas] 9[. The contact surface includes the weld areas, HAZ and base metal. All these surfaces are sanded with sandpaper up to 1200 grit before the corrosion test and then degreased with acetone solution and the remaining surfaces that should not be in the vicinity of the electrolyte solution are insulated with a special varnish.

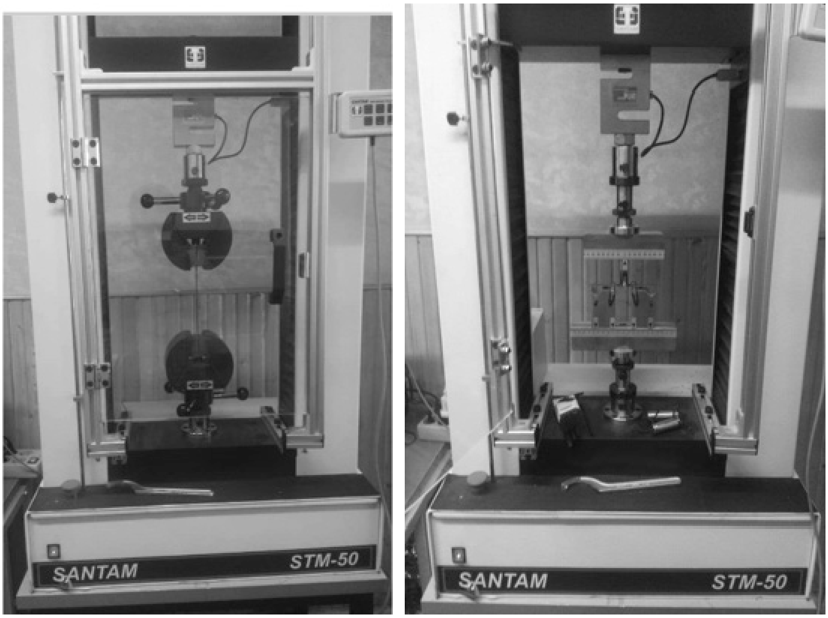

Figure 4- Centam STM 50 device

2-13- Numerical modeling of tensile and bending tests

In this study, two tensile and bending tests were numerically modeled based on the finite element method. For this purpose, Abaqus 2022 software was used. In order to model a problem in the Abaqus environment, different modules have been considered, each part of the modeling is defined separately in its own module and the modeling is completed based on that.

1- Part module: In this section, the schematic of the steel and the weld area are designed as two separate parts. For this purpose, and based on the exact dimensions and sizes of the welded samples, the weld area and the base metal were designed.

2- Property module: In this module, all the physical and mechanical properties of the components of the model under study will be defined. Considering that the weld material and the base metal material are different, the aforementioned properties were defined for both designed parts in this section. In this study, since each base metal and weld metal are fractured during tensile and bending tests, and this is a deformation in the plastic region, in addition to defining the elastic properties, the plastic properties of the studied materials must also be defined. In order to define these properties, these properties are defined in the Property module from the New option.

3- Assembly module: In this module, the parts designed in the previous section are connected together and show the overall structure of the designed weld. In Figure 5, the final model of the designed weld is shown.

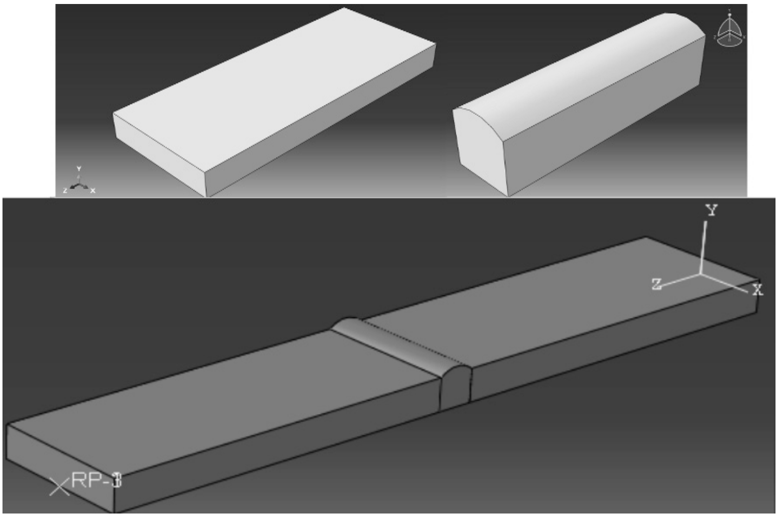

Figure 5-Final designed weld model and its components

4-Step module: In this module, the problem solving method will be defined. The problem under study is of a dynamic type, so for this purpose, the Dynamic Explicit solution method was selected. Due to the high volume of calculations in this modeling, it is necessary to define the method in the Edit section and select the Factor index as 1000 from the Mass Scaling sub-category. This number was selected as a trial and error method so that convergence in solving the problem can be observed in the shortest possible time.

5-Interaction module: In this section, the connection between different surfaces in the designed weld model must be defined. Given that in this research, two steel base metals must be fixed around the designed weld model, in this case, two constraints called Tie must be defined to connect the surfaces of the weld model together. This definition is the same for both tensile and bending tests] 3[, as shown in Figure 6, the process of defining the connection between the base metal and weld surfaces.

On the other hand, for the tensile and bending tests, the load application constraints must be defined separately. In the tensile test, one side of the part is fixed and the other side is under the influence of the tensile force. In order to apply the tensile force to the part, a reference point was defined from the Tools menu and the reference point was connected to the cross-section of the welded part.

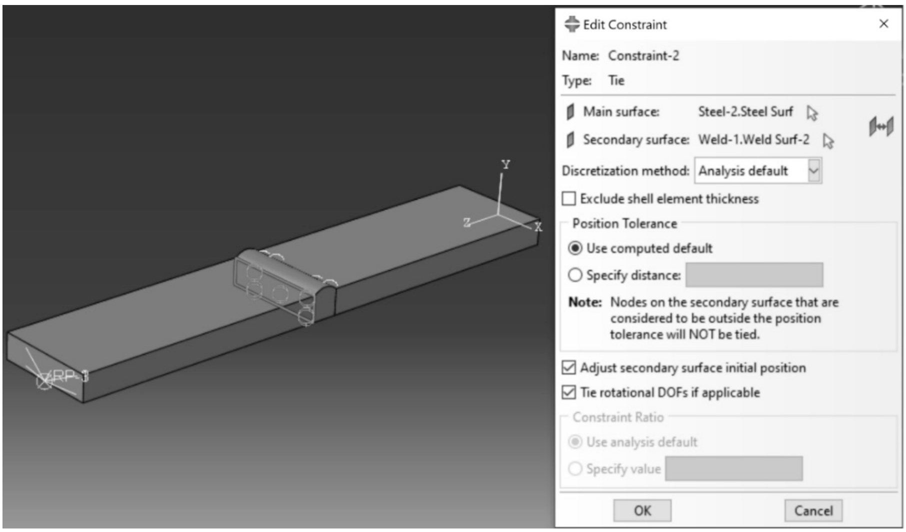

Figure 6-Definition of the relationship between weld plates and base metal with the Tie constraint

In Figure 7, the relationship between the reference point and the cross-section in the tensile test is shown. However, in the bending test, a third part was designed and the force application operation was performed by this part. In Figure 8, the relationship between the bending part and the weld is shown. For this case, a reference point was also defined and the reference point was connected to the effect surface of the bending part.

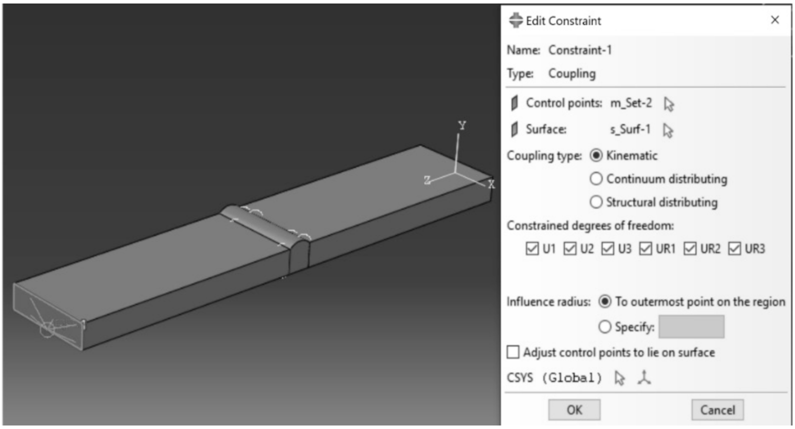

Figure 7-Definition of the relationship between tensile force and weld sample with the Coupling constraint

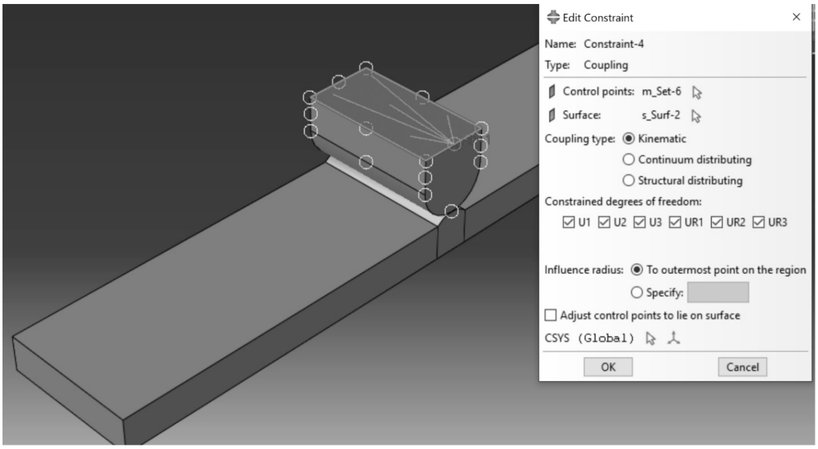

Figure 8-Definition of the relationship between bending force and weld sample with the Coupling constraint

6- Load Module: In this section, only the supports of the weld model are defined. In the tensile test mode, the support was welded with zero degrees of freedom on one side of the specimen. To define the support in the bending test, the supports were defined as zero degrees of freedom on both sides of the weld specimen.

7- Mesh Module: In this module, the research problem is divided into fine components, which is called meshing. In this mode, first select the designed part, then select the selected mesh type as Explicit Mesh. In the meshing settings section, the mesh size can be adjusted, and in this study, the mesh size for the weld area was considered finer than the base metal area. In Figure 9, the final meshed model for the bending test is shown. The meshed models for the bending and tensile tests are similar, and the only difference is the bending element, which is absent in the tensile model.

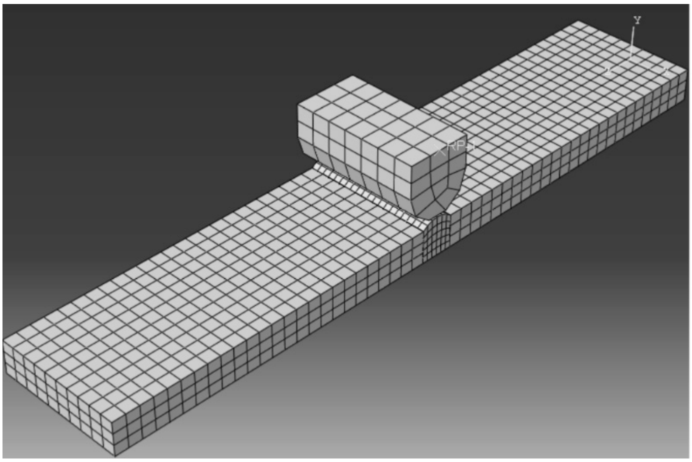

Figure 9-Final meshed model

8-Job and Visualization module: In the Job module, a new problem will be defined and by submitting it, the software will start solving the problem. Then, after solving the problem and completing the solution process, the results of the problem and modeling can be seen in the Visualization module.

2-14- Final analysis

In order to investigate the effect of the type of nanoparticle and its concentration on the mechanical properties, corrosion and percentage of weight loss of the samples, the analysis of variance test with a randomized factorial design with three replications was used. Also, to compare the average effect of the type and concentration of nanoparticles on the above properties, the mean comparison method using the Duncan multiple range test was used. SPSS software was used to analyze the data in this section.

3-Results and Discussion

3-1- Examination of the microstructure of different weld areas

The microstructure of the welded sample without the presence of nanoparticles and with the presence of nanoparticles was examined in this section. Optical and electron microscope images were prepared from different weld areas, including the weld button, the weld-affected area, and the base metal area. Figure 10 shows optical microscope images and electron microscope images for different weld areas without the presence of nanoparticles. Examination of the optical microscope images shows that the average grain size of the base metal is about 10 microns, which is ferrite. The results also show that the grain size in the base metal is larger than the weld button, but the shape of the grains in the weld button is more elongated than the base metal. The increase in temperature in the weld button area causes the grain size to become smaller, and for this reason the grain size in the weld button is larger than the base metal. In simpler terms, in the weld button, due to the high temperature of the molten area, the grains have recrystallized and their size has been elongated, while in the base metal, the recrystallization process has not been performed. Comparison and examination of the light microscope and SEM images showed that there is not much difference in the weld-affected area with the base metal, but in the weld-affected area, the grain size was smaller than the base metal and the grains were more elongated in this area. Examination of the images showed that the grain size in the base metal is more uniform and almost the size of most grains is the same, while moving towards the weld button, this uniformity decreases and the grain size is non-uniform, which is due to the high temperature in the weld button and recrystallization] 10[.

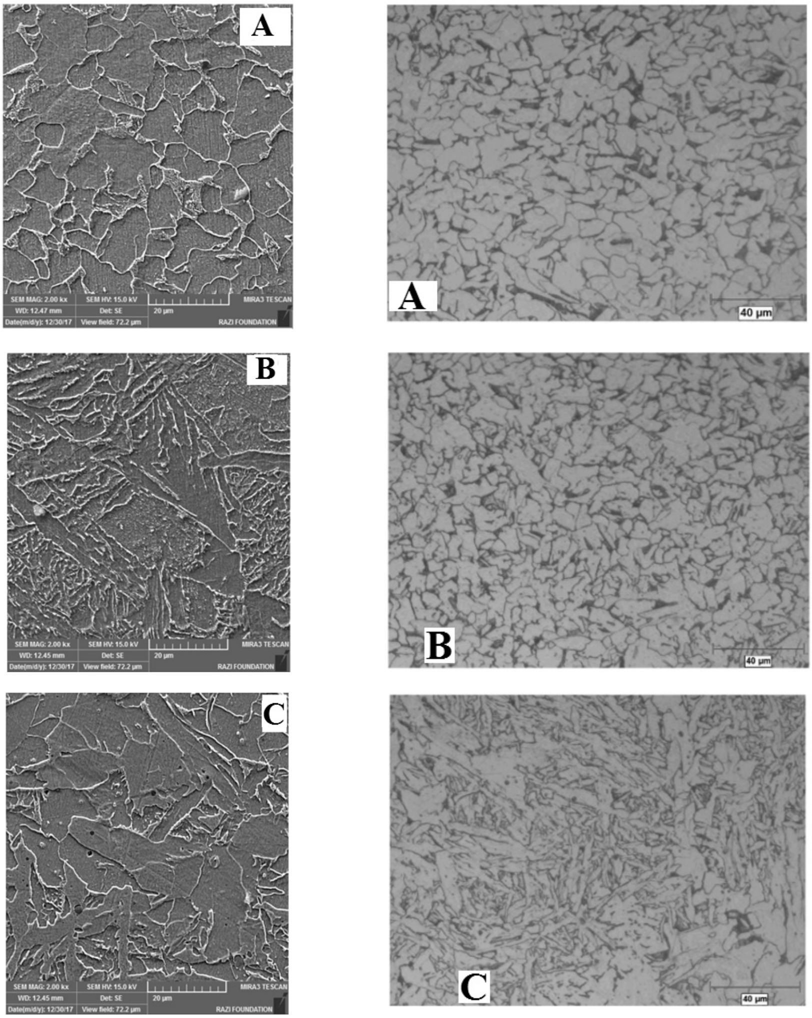

Figure 10- Right: Light microscope images. Left: SEM images of different weld areas (a- base metal, b- weld affected area, c- weld button)

3-2-Study of sample weight loss

In this study, the effect of nanoparticles and their concentration on the percentage of weight loss of the samples was studied. Each sample was weighed before the start of the test. Then, after leaving the tank, it was cleaned by sandblasting and washed with ethanol, and then its final weight was recorded. Then, the percentage of weight loss of the samples was calculated. The percentage of weight loss in this study was calculated for different welded samples with different weight percentages and types of nanoparticles. Table 4 presents the results of the analysis of variance of the effect of nanoparticle type, nanoparticle concentration, and their interaction effects on the percentage of weight loss of the samples. The results showed that firstly, the effect of repetition on the percentage of weight loss had no significant effect, and secondly, both the type of nanoparticle and the concentration, as well as their interaction effects, had an effect on the percentage of weight loss of the samples at the 99% probability level.] 11[

Table 4- Comparison of the average effect of nanoparticle type and concentration on the percentage of weight loss of welded samples

Dependent Variable: WR					
Source	Type III Sum of Squares	df	Mean Square	F	Sig.
Corrected Model	34.978[a]	7	4.997	146.852	.000
Intercept	110.113	1	110.113	3236.074	.000
Rep	.054	2	.027	.790	.480
NanoType	.474	1	.474	13.921	.004
NanoCon	29.664	2	14.832	435.899	.000
NanoType * NanoCon	4.786	2	2.393	70.332	.000
Error	.340	10	.034		
Total	145.431	18			
Corrected Total	35.318	17			
a. R Squared = .990 (Adjusted R Squared = .984)					

Table 5 presents the results of the comparison of the means to select the best method for having the minimum weight loss based on the Duncan method .] 5[The lowest percentage of weight loss was observed for the sample welded with 2.5% titanium dioxide nanoparticles. The weight loss rate in this case was 0.23%. For both nanoparticle samples, with increasing nanoparticle concentration, the percentage of weight loss decreased and then increased. The weight loss rate for both nanoparticles was the highest weight loss in the sample with 1% nanoparticles. Examining the effect of the type of nanoparticle also showed that the effect of TiO2 nanoparticles on reducing corrosion and reducing the percentage of weight loss was greater than that of SiO2 nanoparticles. By changing the concentration of SiO2 nanoparticles to more than 1%, the difference between the percentage of weight loss was not significant. The highest weight loss was observed in the sample containing 1% TiO2 nanoparticles at 54.4%. With increasing nanoparticle concentration, initially the presence of nanoparticles between the grain boundaries prevented corrosion from intensifying, but for higher amounts of nanoparticles, they became clumped and caused holes between the grains, which was the reason for the greater weight loss of the samples.

Table 5- Comparison of the average effect of nanoparticle type and concentration on the percentage of weight loss of each sample

NanoType	Nano Concentration (w%)	Weight Reduction (%)
TiO2	1.0	4.5400[a]
	2.5	0.2300[d]
	5.0	2.1633[c]
SiO2	1.0	3.8333[b]
	2.5	1.9633[c]
	5.0	2.1100[c]

Common letters in each column indicate no significant difference between them.

Figure 11 shows the difference in weight loss for samples containing nanoparticles compared to samples without nanoparticles. An examination of these results shows that using nanoparticles can greatly improve the weight loss rate, so that when using 2.5% TiO2 nanoparticles, the percentage of sample mass loss has improved by about 97.8% compared to the sample without nanoparticles. In general, an examination of the results of this section showed that due to the presence of nanoparticles in the welding process, the weight loss rate of the samples has decreased, which shows the role of nanoparticles as a protective factor against corrosion by gases inside the tank. According to the examination of the weight loss results, the effects of adding TiO2 nanoparticles were more significant compared to SiO2 nanoparticles; therefore, the effect of titanium dioxide nanoparticles on the corrosion and mechanical properties of the weld was investigated.

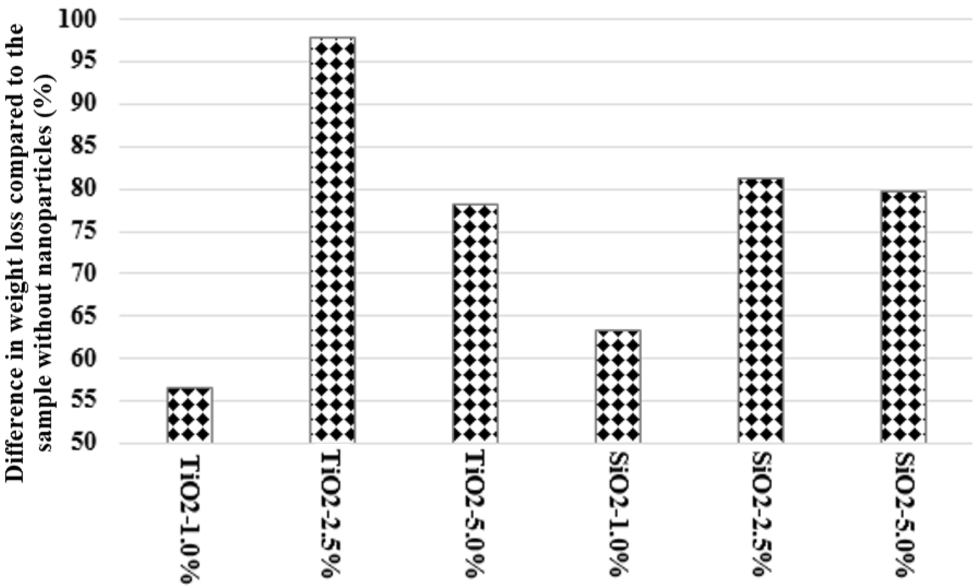

Figure 11-Difference between percentage weight loss for samples containing nanoparticles and samples without nanoparticles

3-3- Investigation of corrosion rates of samples

In this section, the results of the polarization corrosion test for 4 different samples are reported. Table 6 presents the results of the TOEFL corrosion test for potential values and corrosion current intensity. Examination of the results of this table showed that the highest corrosion rate, which is also described by corrosion current intensity, is related to the welded sample without nanoparticles. The corrosion current intensity in this case is 1.03 mA/cm2, which is a significant difference compared to the welded samples with the presence of nanoparticles. With increasing the concentration of titanium dioxide nanoparticles in the welding process, the corrosion current intensity decreased and increased. The lowest corrosion current intensity was observed when using 2.5% nanoparticles. Comparing the corrosion current intensity for concentrations of 1%, 2.5% and 5% with the sample without nanoparticles showed that the corrosion rate decreased by 87.38%, 97.38% and 95.92%. The difference between the percentage of corrosion rate reduction for the 2.5% and 5% samples was not significant. Overall, the results of this section showed that the presence of nanoparticles in the welding process improved the corrosion properties of welded joints, which was also proven in the previous section. The best case in this section for recommending welding is the use of a filler containing 2.5% titanium oxide nanoparticles, which had a significant effect on reducing the corrosion intensity in the samples.

Table 6- Results of the polarization corrosion test for different samples

Label	Corrosion potential E_{corr}(V)	Corrosion current density I_{corr}(mA/cm^2)
Without Nano	-0.454	1.03
1.0 % TiO2	-0.321	0.13
2.5 % TiO2	-0.326	0.027
5.0 % TiO2	-0.331	0.042

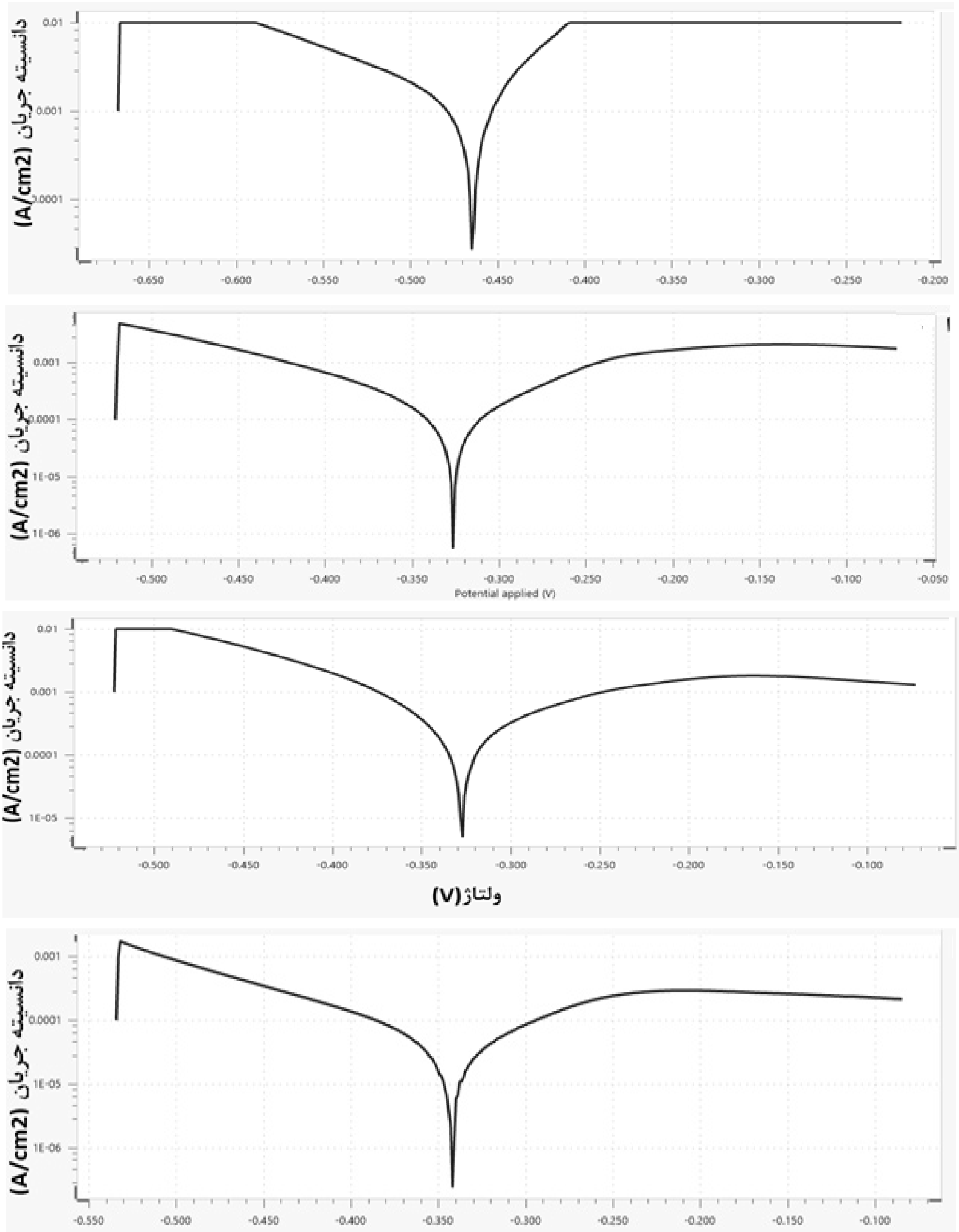

Figure 12- Corrosion test results for different samples containing TiO2 nanoparticles (from top to bottom for samples containing 0%, 1%, 2.5% and 5%, respectively)

3-4- Tensile and bending test results

Figure 13 shows the results of the three-point bending test in the form of stress-strain curves for different welded samples for different concentrations of TiO2 nanoparticles. Examination of the stress-strain curves showed that with the addition of TiO2 nanoparticles, the flexural strength and lateral strain of the samples underwent significant changes. As also shown in the metallographic image analysis section, with the addition of 2.5% TiO2 nanoparticles to the weld, the grain size became finer, which improved the mechanical properties of the studied samples. The results show that in the absence of TiO2 nanoparticles, the maximum flexural strength of the samples was 35.86 MPa, and with the addition of 1%, 2.5%, and 5% TiO2 nanoparticles, the flexural strength was 38.73 MPa, 40.33 MPa, and 40.02 MPa, respectively. The results of the flexural test showed that the addition of 1%, 2.5%, and 5% TiO2 nanoparticles during welding improved the maximum flexural strength of the samples by 8%, 11.17%, and 10.74%.

The results of the uniaxial tensile test are presented in the form of stress-strain curves in Figure 14. Examination of the stress-strain curves showed that by adding different concentrations of nanoparticles to the weld, the ultimate tensile stress increased, while the axial strain decreased. A comparison of the average maximum tensile stress of the samples showed that in the absence of nanoparticles, the maximum tensile strength of the sample was 15.534 MPa, which increased by 6.86%, 9.93%, and 8.80% with the addition of 1%, 2.5%, and 5% TiO2 nanoparticles, respectively.

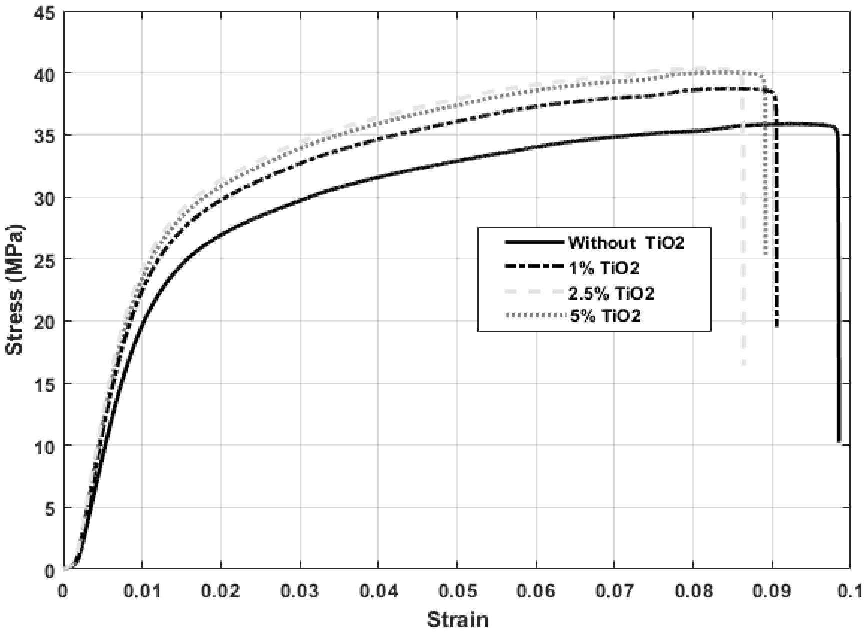

Figure 13- Three-point bending stress-strain curve for samples reinforced with different concentrations of TiO2 nanoparticles

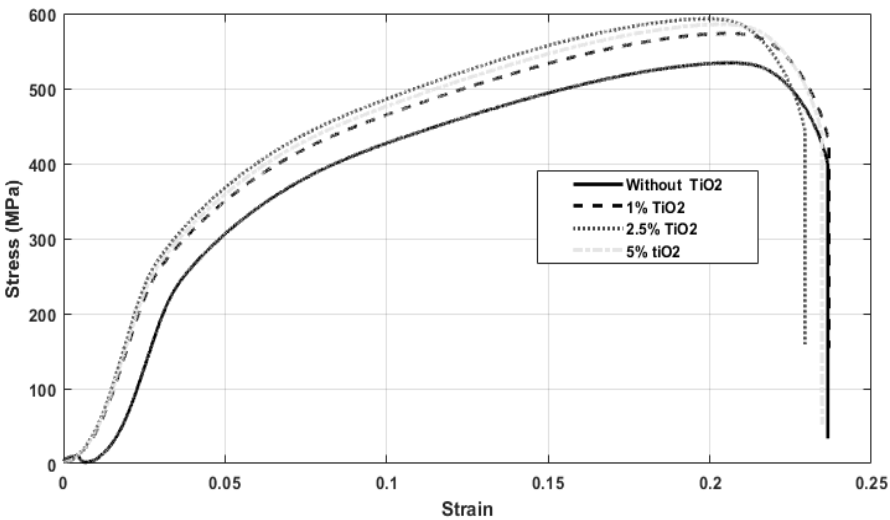

Figure 14-Tensile test stress-strain curve for specimens reinforced with different concentrations of TiO2 nanoparticles

3-5- Numerical modeling results of tensile and bending tests

Figure 15 shows the results of finite element modeling of the bending test for the welded specimen. As can be seen in the figure, the modeled specimen was bent by moving the mandrel downwards and the modeled part did not break during the bending process.

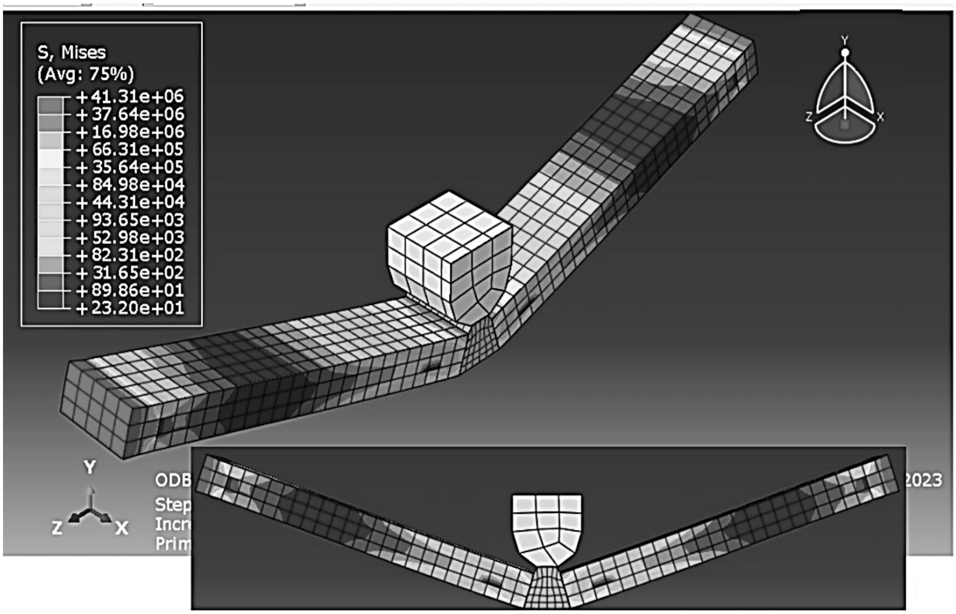

Figure 15- Numerical modeling results of bending test

Figure 16 also shows the experimental bending test result for the specimen. As can be seen in the figure, the bent model and the experimental model were similar and in both models, the failure process did not occur in the part. Examination of Figure 16 showed that in the three-point bending test, the maximum stress occurred at the weld and steel plate junction, or the area affected by the weld, and also at the supports. The maximum bending stress in the modeled sample was 41.31 MPa, while the maximum stress in the experimental sample was 35.86 MPa.

An examination of the numerical and experimental results shows that 13.19% error was observed between the finite element model and the experimental model, and Figure 17 also presents the stress-strain curve of the bending test for the experimental and numerical models. An examination of this figure shows that the trend of changes in the stress-strain curve for the numerical and experimental models in the bending test is similar, but the stress values in the numerical model are higher than in the experimental model. Overall, a good correlation was observed between the experimental and numerical results for the three-point bending test.

Figure 16- Laboratory sample after bending test

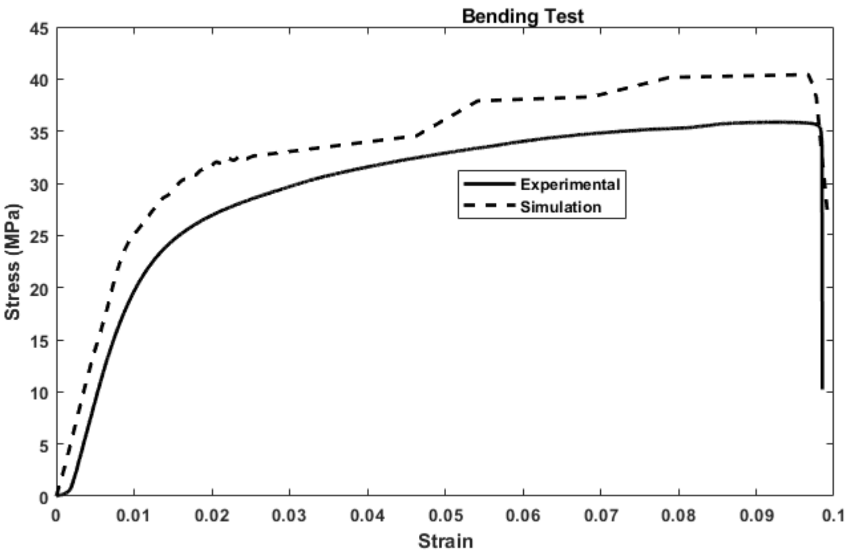

Figure 17- Comparison of stress-strain curve of bending test for experimental and modeled sample by Abaqus

In Figure 18, the modeled finite element model is shown under uniaxial tensile test. Examination of this figure shows that the maximum tensile stress was observed in the weld area and its value was 582.61 MPa, while the actual maximum tensile stress of the experimental sample was 534.15 MPa. The maximum tensile strength for the modeled sample was 9.07% higher than the experimental sample.

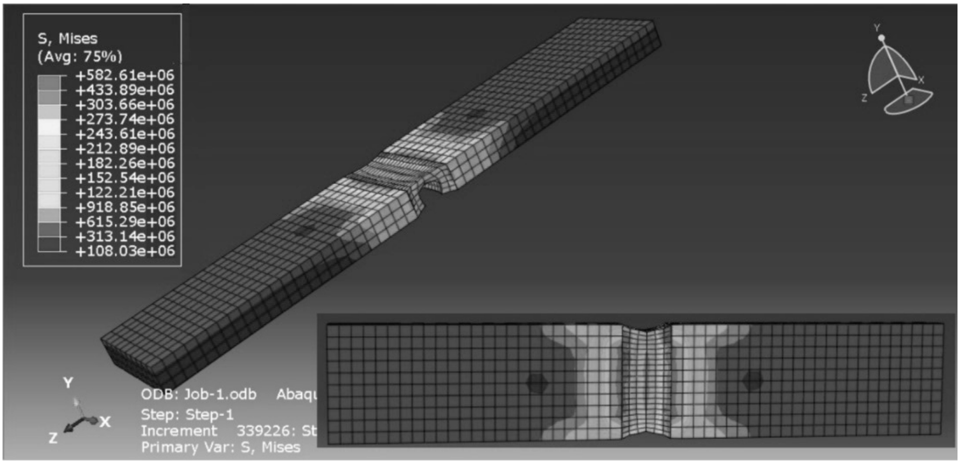

Figure 18-Numerical modeling results of tensile test

In Figure 19, the stress-strain curve for the experimental model and the finite element model under tensile test is shown. In this case, as in the results of the bending test section, the amount of stress that occurred in the modeled sample was higher than the real and experimental model. As in the results shown in the previous sections, some intergranular deposits are formed during welding during welding, and these deposits are important factors in reducing the mechanical properties of the weld. Therefore, the effects of these deposits were ignored during the modeling process, so the final stress value obtained from the numerical models was higher than the real model.

Figure 20 shows the experimental specimen after the tensile test. In this case, the specimen failed near the weld line, which was also the case in the numerical model, but in the numerical model, the failure location was exactly in the middle of the weld line, while in the experimental specimen, the failure location was in the weld-affected area on the tensile force side of the tensioning device.

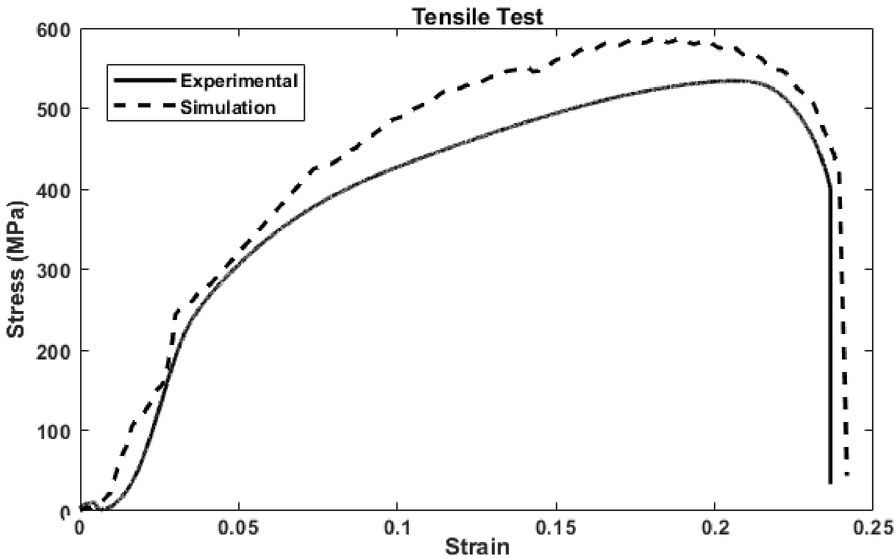

Figure 19-Comparison of tensile test stress-strain curve for experimental and Abaqus modeled samples

Figure 20-Laboratory sample after tensile test

4- Conclusion

In this thesis, the following results were observed:

1. Examination of the microstructure of different parts of the weld line showed that the grain size, grain distribution and uniformity in grain distribution were greater in the base metal area than in the weld-affected area and the weld-affected area than in the weld button area. In the weld button area, the grain size was smaller and the grains were more elongated than in the base metal and weld-affected area.
2. Examination of the weight loss of the welded samples showed that adding nanoparticles during the welding process caused a decrease in the percentage of weight loss. So that for a sample containing 2.5% titanium dioxide nanoparticles, the lowest percentage of weight loss was observed at 0.23%. The results also showed that the effect of titanium dioxide nanoparticles is more effective than silicon dioxide in reducing the weight loss rate.
3. Examination of the corrosion test of the samples showed that with increasing the concentration of nanoparticles in the nanofiller, the corrosion current intensity at the weld site first decreased and then increased. The minimum corrosion current intensity was observed when using nanofiller with 2.5% titanium dioxide nanoparticles. By using nanofillers containing 1%, 2.5% and 5% nanoparticles, the corrosion current intensity at the weld site can be reduced by 87.38%, 97.38% and 95.92%, respectively.
4. Examination of the tensile and bending test results showed that adding TiO_2 nanoparticles during the welding process increased the maximum

flexural and tensile strength of the welded samples, so that for the sample with 2.5% nanoparticles, the maximum flexural and tensile strength increased by 10.74% and 9.93%, respectively.

5. Comparison of numerical and experimental modeling results showed that the error of numerical modeling using the finite element method in measuring tensile and flexural strength was 13.19% and 9.07%, respectively.

5- References

[1] UNESCO. (2011). *Recommendation on the Historic Urban Landscape*. UNESCO World Heritage Centre. https://whc.unesco.org/en/hul/?utm

[2] Bandarin, F., & van Oers, R. (2012). *The historic urban landscape: Managing heritage in an urban century*. Wiley Blackwell, 2012, 236 pp. 75-111p, colour photos, ISBN 978-0-470-65574-0 https://onlinelibrary.wiley.com/doi/book/10.1002/9781119968115?utm_source=chatgpt.com

[3] Pacione, M. (2003). *Urban environmental quality and human wellbeing—A social geographical perspective. Landscape and Urban Planning*, 65(1–2), 19–30. https://doi.org/10.1016/S0169-2046(02)00234-7

[4] Marans, R. W. (2012). Quality of urban life studies: An overview and implications for environment–behaviour research. Procedia – Social and Behavioral Sciences, 35, 9–22. https://doi.org/10.1016/j.sbspro.2012.02.058

[5] Labadi, S., & Logan, W. (2015). *Urban Heritage, Development and Sustainability.* Routledge. https://www.taylorfrancis.com/books/edit/10.4324/9781315728018/urban-heritage-development-sustainability-sophia-labadi-william-logan?utm_source=chatgpt.com

[6] Matthias R., Christer G., Zachary J., Sushobhan M. and Manal G. (2025) Historic Urban Landscapes and Heritage Systems as the Basis for Sustainable Urban Development, *14*(9), 1783;https://doi.org/10.3390/land14091783

[7] Gehl, J. (2011). *Life between buildings: Using public space* (6th ed.). Island Press.

[8] Carmona, M. (2019)Principles for public space design, planning to do better. *Urban Des Int* 24, 47–59. https://doi.org/10.1057/s41289-018-0070-3

[9] Rypkema, D. D. (2005). *The economics of historic preservation*. National Trust for Historic Preservation.

[10] Pendlebury, J. (2013). Conservation values, the authorised heritage discourse and the conservation-planning assemblage. *International Journal of Heritage Studies*, *19*(7), 709–727. https://doi.org/10.1080/13527258.2012.700282

[11] Graham, B., Ashworth, G. J., & Tunbridge, J. E. (2000). *A geography of heritage: Power, culture and economy*. Arnold.

[12] UN-Habitat. (2015). *Global public space toolkit: From global principles to local policies and practice*. United Nations Human Settlements Program.

[13] Jamal A. Measuring Quality of Life in Urban Areas: Toward an Integrated Approach. Int J Environ Sci Nat Res. 2020; 25(2): 556158. DOI: 10.19080/IJESNR.2020.25.556158

[14] Hillier, B., & Hanson, J. (1984). *The social logic of space*. Cambridge University Press.

[15] Hillier, B. (2007). *Space is the machine: A configurational theory of architecture*. Space Syntax.

[16] Yin, R. K. (2018). *Case study research and applications: Design and methods* (6th ed.). SAGE Publications.

[17] Groat, L., & Wang, D. (2013). *Architectural research methods* (2nd ed.). John Wiley & Sons.

[18] Likert, R. (1932). *A technique for the measurement of attitudes*. Archives of Psychology, 140, 1–55.

[19] Whyte, W. H. (1980). *The social life of small urban spaces*. Project for Public Spaces.

[20] Creswell, J. W. (2014). *Research design: Qualitative, quantitative, and mixed methods approaches* (4th ed.). SAGE Publications.

[21] M. S. Ibrahim and A. I. Altif, (2017) “Architectural Elements in Mustansiriyah Madrasah in Baghdad,” Al MalweahArchaeol. Hist. Stud., vol. 4, no. 7, pp. 253–282, 2017 *(PDF) Sustainability Investigation of the Old Mustansiriya Madrasa in Modern Construction: A Comparative Study*. Available from: https://www.researchgate.net/publication/393209498_Sustainability_Investigation_of_the_Old_Mustansiriya_Madrasa_in_Modern_Construction_A_Comparative_Study [accessed Jan 16 2026].

[22] Abdulrahman, M. @mustafa. bdulrahman (2025, اوكتوبر 03). *صورة جوية للفناء أثناء الفعالية المسائية في المدرسة المستنصرية [صورة]*. Instagram. https://www.instagram.com/mustafa.bdulrahman/